Silicon (2022) 14:11805–11820
https://doi.org/10.1007/s12633-022-01901-6

ORIGINAL PAPER

Influence of Dual Range Particle Size on Wear and Friction Properties of Ilmenite Reinforced Aluminium Metal Matrix Composite

Varun Singhal [1,2] · O. P. Pandey [1]

Received: 27 January 2022 / Accepted: 18 April 2022 / Published online: 29 April 2022

Abstract

The present work has been taken to develop aluminum matrix composites (AMCs) for break drum application. Currently, cast iron is used to fabricate brake drums in various automobile industries. In this study, the composite was developed using Al-Si alloy (LM30) as a matrix and ilmenite mineral as a reinforcement. The stir casting process was used to synthesize the composites with ilmenite reinforced particles having two different particle sizes (fine: coarse; F-32-50 μm, C-75-106 μm). The particle distribution, hardness, wear, and load-structural relationships have been studied for all the developed composites. The best wear resistance was observed for 15 wt% ilmenite reinforced (4:1; fine: coarse ratio) composite. This has shown an improvement in wear resistance up to 57%, whereas the coefficient of friction was considerably reduced up to 47% compared to LM30 (Al-Si alloy) sample. To check the industrial sustainability of the prepared samples, the wear analysis of the composites was also compared with the gray cast iron. For the brake drum application, aluminium metal matrix composites showed ~ 6% more wear loss than that of cast iron. The wear track/debris micrographs indicated that the abrasive wear mechanism was prevalent. A significant plastic deformation with increased contact pressure of 1.4 MPa is observed. This has led to generation of micro cracks followed by material removal with increased pressure.

Keywords Wear · Coefficient of friction · Tribo-layer · Ilmenite

1 Introduction

The requirement for lightweight wear resistance materials for automobile application is increasing. This demand is currently addressed by a new class of composites containing a wide range of reinforced particles. This helps to support the applied load over a long time by transferring the load from bigger reinforced particles to smaller ones, thus protecting the matrix from further wear. Although fine particles provide excellent wear resistance but these fine particles have a tendency to segregate. In order to keep them separated a blend of two different sized particles were taken which help to disperse fine-particles and agglomeration is avoided. This arrangement helps to strengthen the matrix.

Generally, hypereutectic Al-Si alloy is reinforced with natural or synthetic ceramics particles. This alloy has a low density and good thermal conductivity [1, 2]. The composite containing synthetic ceramic particles like SiO_2 [3], ZrO_2 [4], SiC [5], B_4C [6], Al_2O_3 [7], etc. and also natural ceramic particles like sillimanite [8], rutile [9], garnet [10] and zircon [11], etc. have been developed and studied. Synthetic ceramic is expensive, thus raising the price of AMCs. Instead of this, natural ceramics particles are economical and easily available. Mineral reinforced composites have shown comparable mechanical and physical properties. Even in some cases it has shown better properties as compared to synthetic ceramic reinforced composites [12]. Moreover, such composites are less expensive than synthetic ceramics reinforced composites [12–15]. These reinforced particles in the Al-alloys improve the hardness, wear property, and thermal property of the AMCs [8, 16, 17].

Many studies pertaining to incorporating natural ceramic particles like sillimanite (Al_2SiO_5), rutile (TiO_2), etc., to improve the wear resistance of Al alloys have been reported

✉ O. P. Pandey
oppandey@thapar.edu

[1] Metallurgy Lab, School of Physics and Materials Science, Thapar Institute of Engineering and Technology, Patiala 147004, Punjab, India

[2] Mechanical Engineering Department, IMS Engineering College, Dasna, Ghaziabad 201001, Uttar Pradesh, India

[18–22]. The research groups have also studied a different range of particle sizes of sillimanite and observed that the particle size significantly affects the wear properties of the AMCs. The interfacial strength between the reinforcement and the Al matrix is significant in improving the wear resistance of aluminium metal matrix composites (AMCs) [23]. If such interfacial strength is weak, the voids are generated, resulting in crack formation. Voids present in the composite also decrease the load-carrying ability of particles and reduce the wear resistance of AMCs. Therefore, to further improve the wear resistance of AMCs, solid interfacial strength is essential. The natural ceramics particle-like Al_2SiO_5, TiO_2, ZrO_2, etc., have superior interfacial strength with the Al-matrix.

The natural mineral ilmenite (density 4.7gm/cc) is crystalline iron titanium oxide ($FeTiO_3$). It belongs to a group of titanium-containing ceramics. Ilmenite is plentifully accessible in the seaside zone of Orissa, Tamil Nadu (India). Ilmenite is a high strength, corrosive resistant, and isotropic material. As per the report of Rasidhar et al. [24] and Elwan et al. [25], the addition of $FeTiO_3$ mineral into the Al-Si alloy enhanced the mechanical properties of composites. $FeTiO_3$ formed a secondary phase $FeAl_3$, which opposes dislocation development inside the Al-matrix and is more resistant to applied loads. Arora et al. [9] and Kumar et al. [19] observed that using rutile (TiO_2) mineral (reinforcement) improves the wear resistance of produced AMCs by refining the Si phase existing in the Al-Si base alloy. As per the available literature, the natural mineral particle reinforced AMCs have shown better higher wear resistance as compared to pure ceramic reinforced composites. Previously, we reported the impact of single range ilmenite reinforced (106 − 75, 75 − 50, and 50 − 32 μm) composites with varying concentrations (5, 10, 15, and 20 wt%) on the wear behaviour of the composites [26]. The wear study reveals that the 15 wt% reinforcement (50 − 32 μm) ilmenite reinforced composite has shown improved wear resistance up to ~ 50% and 55% at 0.2 MPa and 1.4 MPa contact pressures, respectively [26]. When the concentration of fine particle ilmenite is increased above the 15 wt%, it shows segregation in the Al-matrix, which affects the wear properties of AMCs [26]. So, reinforcing the dual-range of ilmenite to develop the AMCs is required to enhance the wear resistance, which has not been reported yet.

In the present work, composite containing ilmenite minerals have been developed. Dual-range particle size (DRP) ilmenite particles have been reinforced in the matrix of LM30 aluminium alloy. The wear behaviour of all composites was investigated and compared to that of cast iron utilized in the automotive industry. Finally, SEM-EDS analysis of worn surface/debris has been done to establish a link between wear outcomes and wear mechanism.

2 Experimental Procedure

2.1 Materials

For the fabrication of AMCs, hypereutectic Al-Si alloy (LM30) (EMPL, India) and ilmenite minerals (IREL, India) were used. The detailed composition of LM30 Al-alloy, ilmenite, and cast iron are enlisted in Table 1.

2.2 Synthesis of AMCs

2.2.1 Ball Milling of Ilmenite

The planetary ball mill was used for 23–45 h at 283 rpm to reduce the size of the ilmenite powder. The weight ratio of the balls to the powder was 12:1. As shown in the SEM image, the ball-milled particles are of different sizes (Fig. 1). The SEM-EDS analysis of ilmenite particles revels that the Fe, Ti, O are the major elements. Further, ball-milled powders were sieved using sieves of various sizes (125, 106, 75, 50 and 32 μm). Sieving was done at 1 mm, 2 mm, and 3 mm amplitudes in the sieving machine for 90 min at each amplitude to ensure complete sieving.

The powder passed through a 50 μm sieve was collected and named as fine particle size. Further, the powder that went through a 106 μm sieve and remained at a 75 μm sieve is referred as coarse particle size. As per the previous study of Kumar [28] and Sharma et al. [29], the dual particle size fine and coarse have shown improved wear resistance, so in the present investigation, this range was selected. Furthermore, the selected dual-range particles were mixed in the varying concentration of 5–15 wt% in the fine: coarse ratios of 1:4, 2:3, 3:2, and 4:1.

2.2.2 Fabrication Process

To synthesize the AMCs, the sir casting technique was used [29, 30]. Initially, the Al-Si alloy (LM30) billet of 700–800 g was melted in a muffle furnace at 750 °C. Next, the moltenAl-alloy was stirred by a graphite stirrer at 650 rpm. The preheated ilmenite particles (300 °C) were incorporated into the molten alloy after 9 min of stirring. The purpose of the preheating the reinforcement is to eliminate moisture and other volatile substance on the surface of particles. The liquid was then stirred again at 650 rpm for 9 min before being transferred into a prepared cast-iron mold. AMCs were prepared with dual-range particle size ilmenite compositions with fine: coarse ratios as 1:4, 2:3, 3:2, and 4:1. From the developed composites, 8 mm diameter pins as per the ASTM G99-05 norms were prepared from the centre of the casting. The designation of various composite formulations is shown in Table 2.

Table 1 Detail of chemical composition of procured Al-Si alloy (LM30), Ilmenite and Cast Iron

Elements	Concentration (wt%)	Elements	Concentration (wt%)	Elements	Concentration (wt%)
LM30 alloy					
Si	17.7400	Mg	0.5200	Ti	0.0820
Cu	4.1000	Zn	0.2600	Ca	0.0180
Fe	0.5300	Cr	0.0034	Pb	0.0830
Mn	0.1600	Ni	0.0023	Sn	0.0310
Sr	0.0006	Al	Balance		
Ilmenite (wt%)					
TiO_2	55.3	Al_2O_3	0.8	Cr_2O_5	0.1
FeO	20.5	SiO_2	1.6	MgO	1.0
Fe_2O_3	19.9	V_2O_5	0.2		
Cast iron					
Si	1.66	Cr	0.11	S	0.12
Fe	93.77	C	3.52		
Mg	0.72	P	0.10		

2.3 Testing and Characterization

Initially, to investigate the distribution of ilmenite particles inside the Al-matrix, samples were prepared by following the metallographic procedure as per the ASTM E3-11. The prepared samples were examined under the optical microscope ((Eclipse MA-100, Tokyo (Japan)). The bulk hardness of sample was measured using Rockwell hardness tester, model no. TRSND, (India) on the B-scale with 100 kg load with ϕ 1/16' ball indenter for 6 s dwell time. The micro-hardness was measured in the Vickers scale with 100 Kgf load and diamond indenter as per ASTM E-92. For both bulk and micro hardness average of 5 samples for a given condition was taken. The pin on disc tribometer (Wear and Friction Monitor

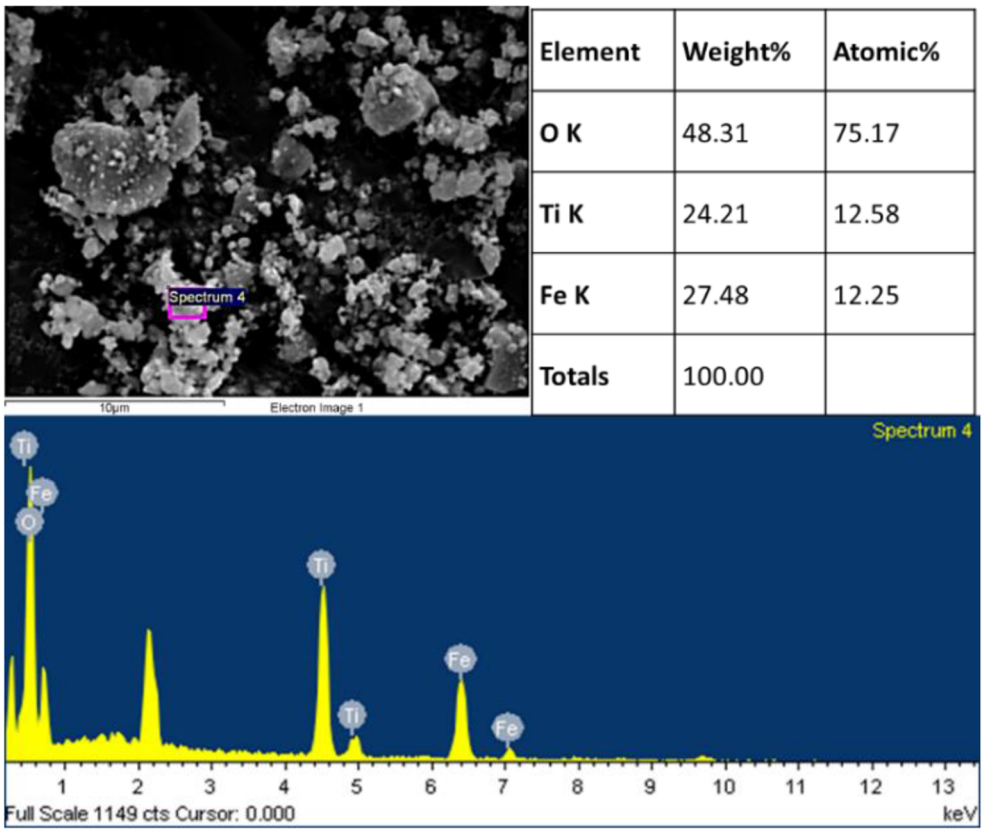

Fig. 1 SEM-EDS analysis of ball-milled ilmenite powder

Table 2 Label used for various manufactured AMCs

	Ilmenite reinforcement in AMCs with fine: coarse ratio			
	1:4	2:3	3:2	4:1
5	5DRP14	5DRP23	5DRP32	5DRP41
10	10DRP14	10DRP23	10DRP32	10DRP41
15	15DRP14	15DRP23	15DRP32	15DRP41

DRP: Dual Range Particles

TR-20, Ducom Instruments, Bangalore (India)) was used for wear test under dry sliding condition. The pin-on-disc test was performed on steel counter surface (EN31 die steel; 831 HV) at constant velocity (1.6 m/sec) at different contact pressures (0.2–1.4 MPa). The relative humidity was between 30 and 35% and the room temperature was 24–28 °C during the wear testing. Further, the total wear loss of the sample in terms of volume is calculated by using $\mathbf{V_T} = \mathbf{H_w} \times \mathbf{A_I}$ (V_T; wear loss, H_W; loss of height, A_I; area of contact ($= \frac{\pi}{4}\boldsymbol{d}^2$), d pin diameter) formula. The height loss was measured from the attached LVDT (± 0.1 μm) sensor in the tribometer. In addition, the wear was determined by using; $\mathbf{W_r} = \frac{\mathbf{V_T}}{\mathbf{D}}$; W_r – Wear rate, D – Sliding distance (= 1.6 × time), and $\mathbf{COF} = \frac{\mathbf{F}}{\mathbf{L}}$; (F – Friction force, L – Normal load). The wear results introduced in this work are an average of three tests performed on four samples for each condition. Moreover, an IR laser thermometer was used to detect the contact temperature during the sliding motion. Worn pin surface and debris was investigated under SEM to establish wear mechanism. The Si size and tribolayer thickness were measured using Image J software.

3 Results and Discussion

3.1 Optical Micrographs

Figure 2(a) displays the microstructure of LM30 Al-Si alloy at 100X magnification. The faceted primary-Si (~ 133 μm) and fine acicular eutectic-Si mixture present in the LM30 alloy are observed in Fig. 2(a). Primary-Si nucleated heterogeneously in Al matrix, with faceted morphology such as cube, star, and polyhedral type. Moreover, the α-Al phase was propagated around the primary and eutectic Si phases. With due course of cooling, oversaturated dissolved Si was precipitated out from the Al phase resulting in the formation of eutectic Al-Si phase as marked in Fig. 2(a) [31, 32]. Coarse primary-Si facets are randomly distributed in the LM30 alloy. This randomly distributed Si phase decrease the wear resistance of the LM30 alloy. The fine and uniformly distributed Si phase is essential for improved wear resistance [33].

Figure 2(b–e) represents the 15DRP14, 15DRP23, 15DRP32, and 15DRP41 composites at 100 X magnification. The coarse and fine size of ilmenite particles is uniformly distributed all over the matrix. Also, secondary Si got transformed from acicular (Fig. 2a) to globular (Fig. 2b-e) form. The melting temperature of ilmenite particles is high, while the thermal conductivity is low (5.25 mcal/ (cm. sec.)) than LM30 alloy. As a result, these ilmenite particles serve as nuclei for molten Al-Si alloy. Therefore, the nucleation of the Si phase has occurred on the surface of ilmenite particles inside the molten alloy (Fig. 2f). It increases the intensity of the silicon phase surrounding the ilmenite particles. The diffusion process begins after solidification. As a result, the silicon far from the particles may also be seen. Ilmenite particles create an obstacle to the diffusion process of Al and Si [8]. The resultant is the refinement of the primary silicon and eutectic Al-Si morphology. It may also be seen from Figure (b-e) that the increase in the concentration of fine particles will provide more nucleation center and help to decrease the size of the primary Si in the sequence of 15DRP14 (64.66 ± 15) > 15DRP23 (58.20 ± 8) > 15DRP32 (56.64 ± 6) > 15DRP41 (33.79 ± 2). The primary silicon size of the 15DRP41 composite was reduced ~ 74% than the base alloy. Figure 2(g) presents the SEM-EDS analysis of prepared composite. It depicts the presence of aluminium, silicon, and oxygen in the ilmenite particles. Further SEM-EDS confirmed the successful inclusion of ilmenite particles in the Al-matrix as shown in Fig. 2(g).

3.2 Hardness Testing

3.2.1 Rockwell Hardness

The hardness of synthesized specimens was measured through the Rockwell hardness machine.

Table 3 exhibited that the bulk hardness of the fabricated AMCs enhanced due to the incorporation of hard reinforcement (ilmenite) in the soft Al-alloy. This increased hardness is due to the Si refinement, which provided barrier for the movement of dislocations generated due to plastic deformation by indenter and hence an increased hardness of AMCs was observed. Moreover, the increased content of reinforcement having more fine size particles also provide hindrance for the dislocation motion causing increased hardness as given in Table 3.

3.2.2 Vicker Hardness Testing

Figure 3a represents the variation in microhardness of different composites at different zones. Microhardness testing was carried out at various phases, such as the Al-matrix (M), ilmenite particles (P), and reinforcement

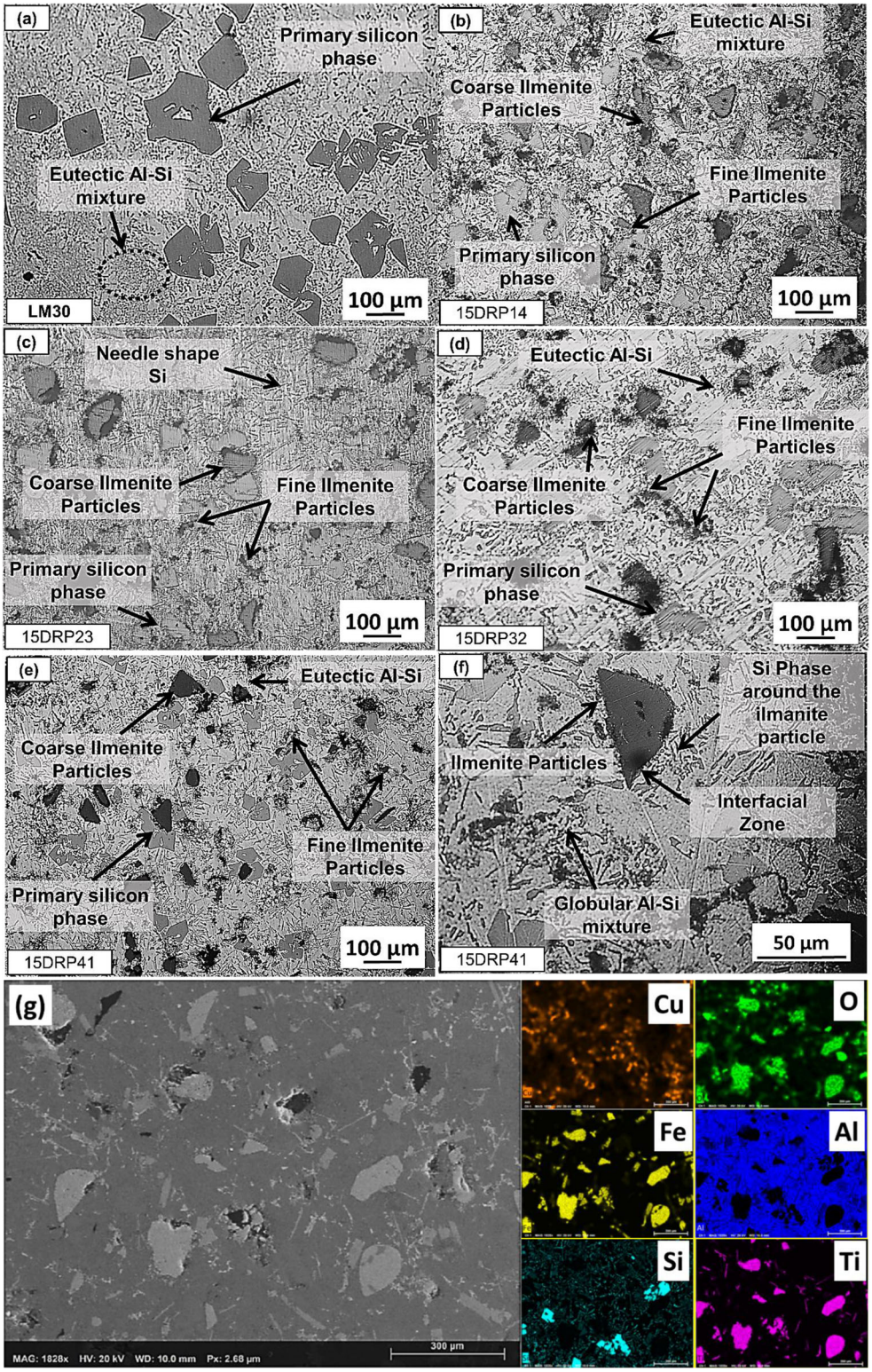

Fig. 2 Microstructure of (**a**) LM30 (Al-Si alloy), (**b**) 15DRP14, (**c**) 15DRP23, (**d**) 15DRP32 (**e**) 15DRP41 at 100X, (**f**) 15DRP41 at 500X magnification and (**g**) SEM-EDS analysis of 15DRP41 composite sample

particle interface (I). The hardness sequence increment was M < I < P as observed from Fig. 3(a). Figure 3(b, c and d) represents an optical micrograph of the indentation mark at different zones, i.e. at matrix, particles and also at the particle-matrix interface, respectively.

The microhardness of the Al-Si alloy is 1.98 Gpa. Moreover, the incorporation of ilmenite particles shows the high microhardness at the particle-matrix interface which shows the strengthing of interfacial bonding. The incorporation of the ilmenite particles increases the dislocation density

Table 3 Rockwell hardness of the LM30 alloy and various AMCs

Sample	Rockwell hardness (HRB)	Sample	Rockwell hardness (HRB)
LM30	75±4	15DRP14	89±6
10DRP14	83±6	15DRP23	91±5
10DRP23	84±8	15DRP32	93±9
10DRP32	86±7	15DRP41	99±3
10DRP41	87±9		

of the AMCs. Moreover, with the increased dislocation density, the AMCs hardness increased. The dislocation density at the composite was determined by using Eq. 1 [34].

$$\rho = \frac{B\varepsilon V_p}{bd(1 - V_p)} \tag{1}$$

Where, B: geometric constant that depends on the aspect ratio (it varies between 4 and 12, it is 4 for whisker-like particulates and 12 for equiaxed particulates), ε: thermal mismatch strain; it is the product of temperature change during solidification of MMCs (δT) and CTE difference between matrix- reinforcement (Δα), Vp: volume fraction of ilmenite reinforcement, b: Burger vector, d: average diameter of reinforcement

Table 4 displays the dislocation density of 15 wt% ilmenite reinforced composites. Sample 15DRP41 showed higher dislocation density than other composite. Therefore, sample 15DRP41 has shown higher hardness among all the fabricated AMCs. The refinement of Si and the presence of a sufficient amount of fine-sized ilmenite particles restricts the spreading path of dislocation in the Al-matrix. Therefore, the AMCs hardness is increased.

3.3 Porosity

Porosity of the AMCs was calculated by using the Eq. 2 as given below.

$$\text{Porosity}(\%) = \frac{\rho_{th} - \rho_{ex}}{\rho_{th}} \times 100 \tag{2}$$

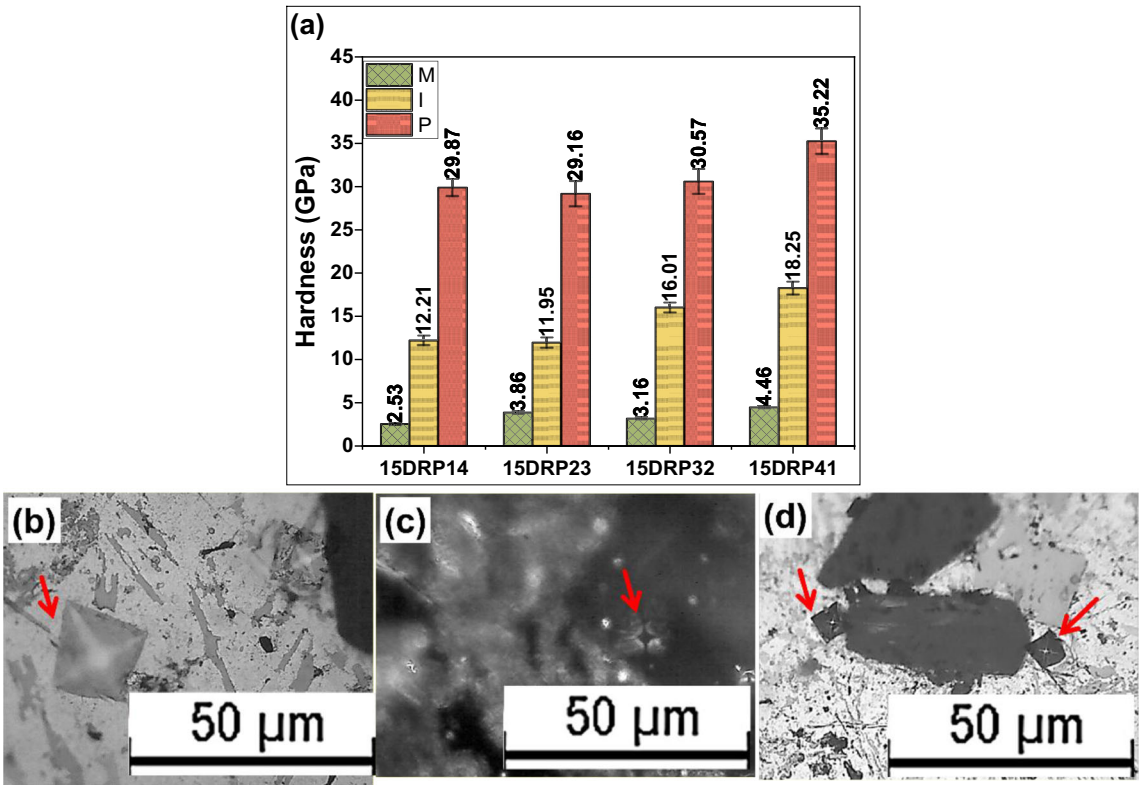

Fig. 3 (**a**) Variation in vicker hardness of different AMCs in different zones and Optical micrograph of micro indentation mark at (**b**) Matrix (**c**) particle and (**d**) interface at same magnification showing variation in indentation size (Marked as an arrow)

Table 4 Dislocation density of different fabricated composite

Sample	B	ε	V_p	b(nm)	d (μm)	ρ ($\times 10^{11}$ m^{-2})
15DRP14	12	0.002827	0.09	0.32	89	11.81
15DRP23	12	0.002827	0.09	0.32	87	12.10
15DRP32	12	0.002827	0.09	0.32	62	16.90
15DRP41	12	0.002827	0.09	0.32	38	27.62

Where ρ_{th}: theoretical density and ρ_{ex}: experimental density

Calculated values are tabulated in Table 5. It is observed that porosity increases with increased content of reinforcement. However, less than 3%, which is negligible [35].

3.4 Contact Temperature

The contact surface temperature between the sample and steel disc is increased during dry sliding under different loading conditions. Figure 4 shows the sliding distance-contact temperature graph. The rise in contact temperature has led to atmospheric chemical reactions and formation of oxide layers on the contact area of the pin surface. These oxide layers restrict the path of the interaction of the pin and counter disc [36]. The temperature rises step by step with sliding distance. At low pressure, this rise is less as compared to high pressure. The friction energy increases as the contact pressure increases. Thus, a larger temperature rise is observed at higher contact pressure. However, increasing the ilmenite particle concentration in the matrix reduced the temperature rise due to the low thermal conductivity of AMCs [30].

3.5 Wear Testing

3.5.1 Effect of Sliding Distance

The wear rate vs. sliding distance curve of samples LM30 alloy, 15DRP14, 15DRP23, 15DRP32, and 15DRP41 are presented in Fig. 5 at (0.2–1.4 MPa) contact pressures. The study of these curves is based on two distinct areas (i) Run in wear and (ii) Steady-state wear. As per the visual observation, in the run-in wear area, the wear rate sharply increased to 250 m. After that, the wear rate declined rapidly up to 1750 m (base alloy) and 1500 m (for AMCs). The sharp increment in wear rate is due to surface asperities interaction with the counter surface. The hard counter surface asperities dig into the soft surface of the pin, causing an abrasion on the pin surface. This abrasion is referred to as plowing action. The pin surface asperities deform with continuous sliding motion, resulting in the development of grooves (abrasive) on the contact surface of the pin. As shown in Fig. 5, the contact temperature increased due to increased contact area. As a result, both the contact surfaces were partially welded to the counter disc. In this order, under the action of forces, these welded joints are plastically deformed and initiate the nucleation of cracks and tearing action from the surfaces in the form of heavy material losses [7, 37]. Thus the wear rate of fabricated base alloy and AMCs increased up to 250 m. But in the AMCs, ilmenite particles inhibit fracture growth and reduce pin surface tearing. Thus the wear rate of AMCs was lesser than that of the LM30 alloy. Beyond 250 m, due to continuing relative motion, the formation of hard oxide film between the pin and counter surface during sliding motion leads to a decrease in the wear rate caused by the oxidation wear mechanism [38]. Hence, the wear rate graph decreases.

Moreover, the wear rate of LM30 and the AMCs becomes more steady, called steady-state wear after certain sliding distance. For the LM30 and AMCs, the steady-state was seen beyond 1750 m and 1500 m, respectively. In the steady-state zone, the high contact temperature leads to oxidation of the pin surface and the formation of an insulating layer.

The protecting layer reduced the interaction between the sample and the steel disc [39]. As a result of pressure and sliding motion, the oxide layer formation and its deformation becomes consistent. As a result, a steady-state wear rate is recorded.

In all fabricated samples, 15DRP41 AMC shows more wear resistance. The addition of ilmenite minerals into the Al-alloy improves the load-bearing strength. The wear strength of the AMCs increased as the fine particle concentration in the fine-coarse particle ratio increased. The coarse particles bear a significant portion of contact pressure in the fine-coarse particle ratio and protect the fine particles and matrix. It improves the load-bearing strength of the AMCs. Due to the continuous action of shear force, a shear force breaks the coarse particles. In the end, the shear force moved on finer particles and the matrix. This provides a higher wear resistance of 15DRP41 AMC, 57% more than the LM30 alloy at 1.4 MPa contact pressure.

Table 5 Variation in porosity of fabricated samples

Samples	Density (g/cm^3)		Porosity (%)
	Theoretical	Experimental	
LM30	2.523	2.511	0.40
15DRP14	2.609	2.581	1.07
15DRP23	2.613	2.558	2.10
15DRP32	2.618	2.550	2.59
15DRP41	2.628	2.548	3.04

3.5.2 Influence of Contact Pressure

Figure 6 depicts the comparative study of the influence of contact pressure for the LM30 and various AMCs

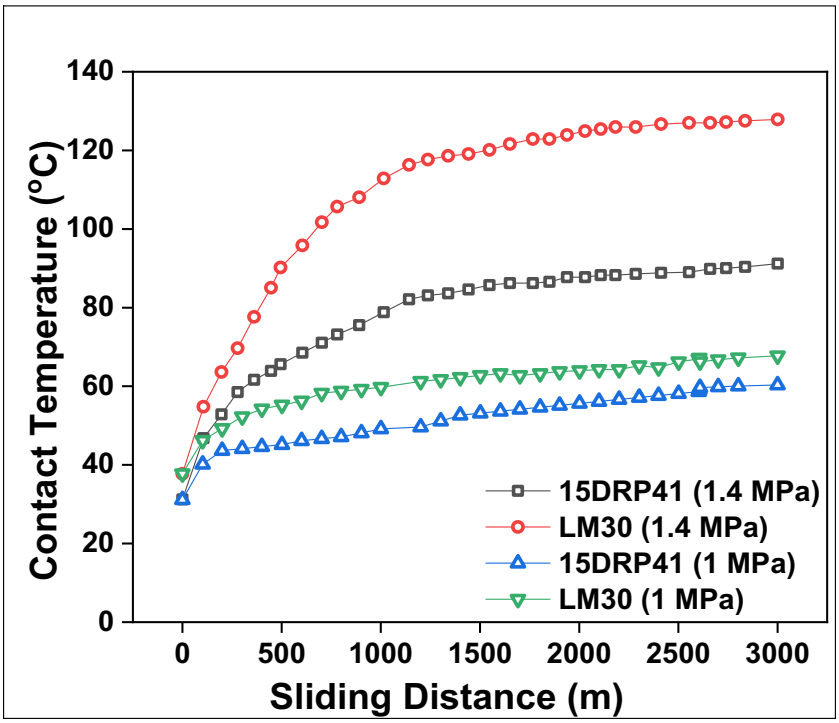

Fig. 4 Varition in contact temperature of base alloy and 15DRP41 during sliding motion at 1 and 1.4 MPa contact pressure

formulations. A linear fitting has been done between the maximum point of wear rate and contact pressure. It can be observed that the wear rate increased with increased contact pressure. At all contact pressure, the slope of the base alloy was higher than the fabricated AMCs due to more friction heat generated between the pin and counter disc with increasing the contact pressure. Accordingly, the pin surface became soft and the new surface was exposed to wear. In addition, the pin surface gets temporary welded to the steel disc surface and the pin surface tears out. Hence, it increases the wear rate by increasing the contact pressure [8, 27]. Moreover, the pin surface undergoes plastic deformation due to increased contact pressure. It increases the probability of micro-crack formation on the pin contact surface, and more material losses under the delamination wear mechanism and increases the wear losses.

3.5.3 Influence of Ilmenite Particles

Figure 6 depicts the wear behavior of the AMCs, which are reduced with the incorporation of ilmenite particles. The wear resistance of the AMCs increases as the fine-coarse particle ratio increases. The reason is that hard ilmenite reinforcement bear the major contact pressure and shield the matrix from wear. In dual reinforcement, fine particles are uniformly distributed. This provides more number of particles capable to bear the applied load. As a result, the load carrier points increase. The particle-particle distance decreases due to the better distribution of fine particles, as seen in Fig. 2e. The presence of coarse particles, help to distribute the fine particles uniformly and segregation of fine particles is avoided. Under continuous action of shear force, the coarse particles are the major load bearing elements. These particles act as asperities and are broken during sliding action. These broken particles are trapped between pin and disk and thus, three body wear occur. In the end, the shear force moves to the matrix through finer particles. Thus, ilmenite reinforcement protects the pin wear losses. In addition, the presence of ilmenite particles, the contact temperature between the pin and counter surface drops down, which diminishes the plastic deformation of the pin surface and decreases the rate of material loss of AMCs samples [40]. In these AMC samples, 15DRP41 AMC has the best wear resistance (57%). The wear resistance of the 15DRP41 sample is 57% more than the LM30 base alloy at 1.4 MPa contact pressure.

3.5.4 Comparative Wear Study

Figure 7(a) represents the wear results of C3-15 [26] and 15DRP41 at 1.4 MPa contact pressure. It was revealed that the wear resistance of the 15DRP41 composite is ~ 12% more than the C3-15 composite.

Further, for the automobile application (brake rotor) approach, a comparative wear study has been done for the cast iron and 15DRP41 sample at a contact pressure of 0.2 MPa and 1.4 MPa (Fig. 7b). The experimental findings show that the wear rate of 15DRP41 composite is ~ 2.981 and ~ 10.510 (10^{-3} mm^3/m) at 0.2 MPa and 1.4 MPa contact pressure respectively, which seems to be < 1% lower than the cast iron

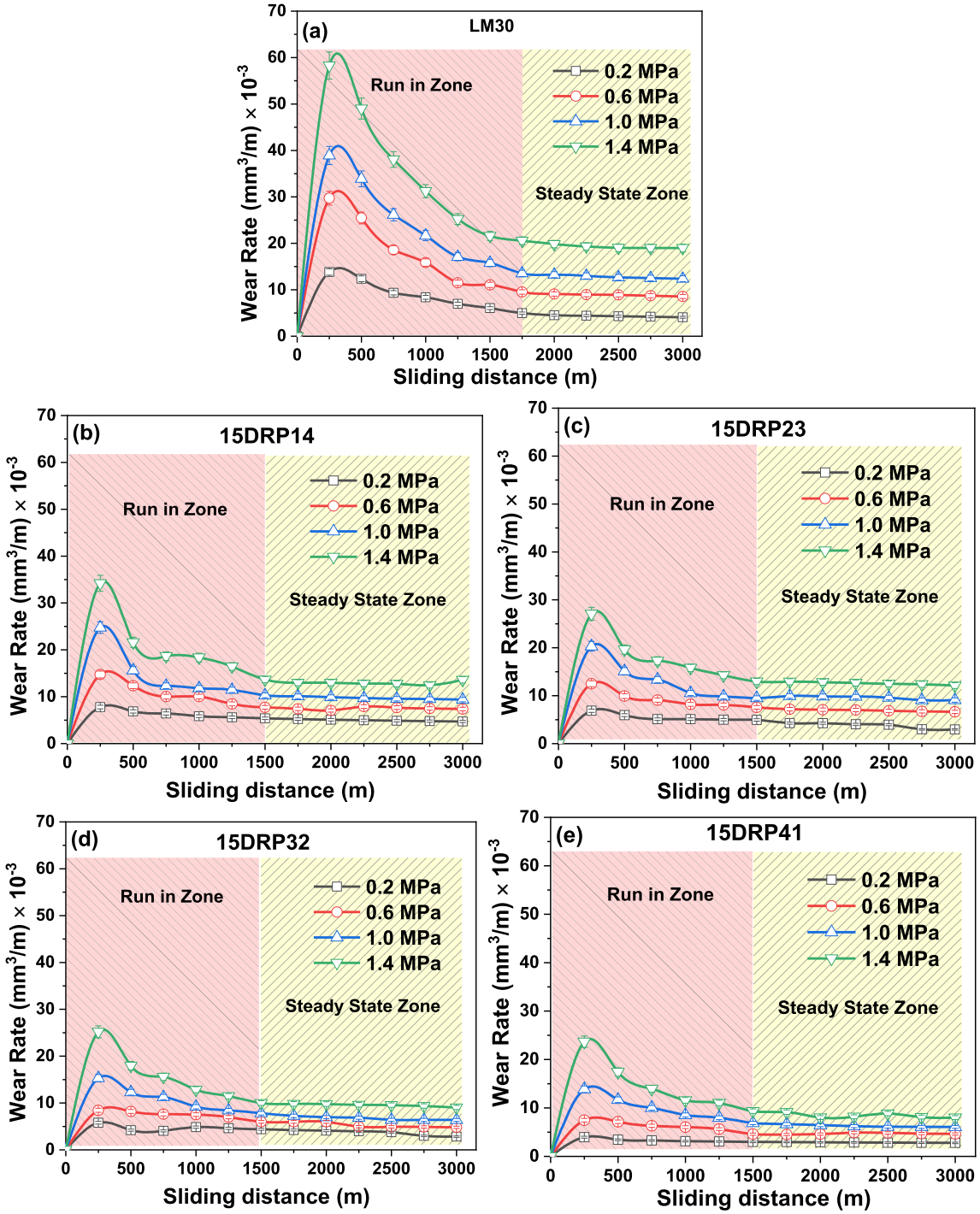

Fig. 5 The variation in wear rate with increasing sliding distance for the fabricated samples

wear rate at 1.4 MPa contact pressure. Also, AMCs fabricated automobile spare parts will be ~ 56% lighter than the components made using cast iron. Considering these facts, composites 15DRP41 seems to be a superior choice for automotive applications.

Moreover, the wear property is superior as compared to similar composite developed in different investigations as shown in the Table 6.

3.6 Coefficient of Friction

The COF curve of Al-Si alloy (LM30) and synthesized composites under different loading conditions and at same sliding distance are displayed in Fig. 8. The COF increased with increased contact pressure, as observed from Fig. 8. Under contact pressure, pin asperity is in contact with counter disc asperity. During sliding motion, the asperity of the counter

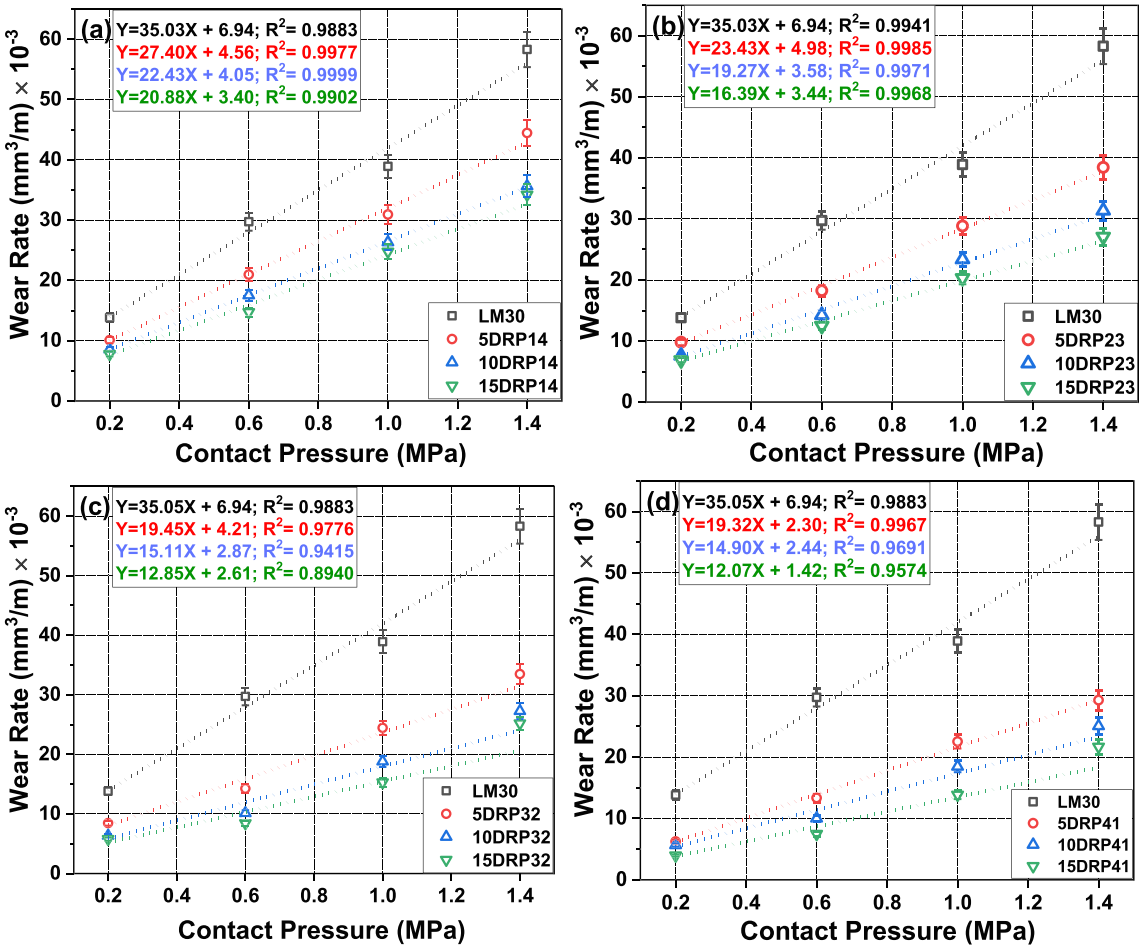

Fig. 6 Maximum wear rate observed at a sliding distance of 250 m for different fabricated samples under different contact pressure conditions

disc penetrates the pin surface with increasing pressure. This deep penetration of counter disc asperity requires more shear forces to continue the sliding movement. The resultant of this is the increased COF [30].

Furthermore, the COF of AMCs dropped as the quantity of fine particles in the selected combination of coarse and fine particles increased. The best result observed is for the 15DRP41 AMC. It shows ~ 46% (at 0.2 MPa) and ~ 41%

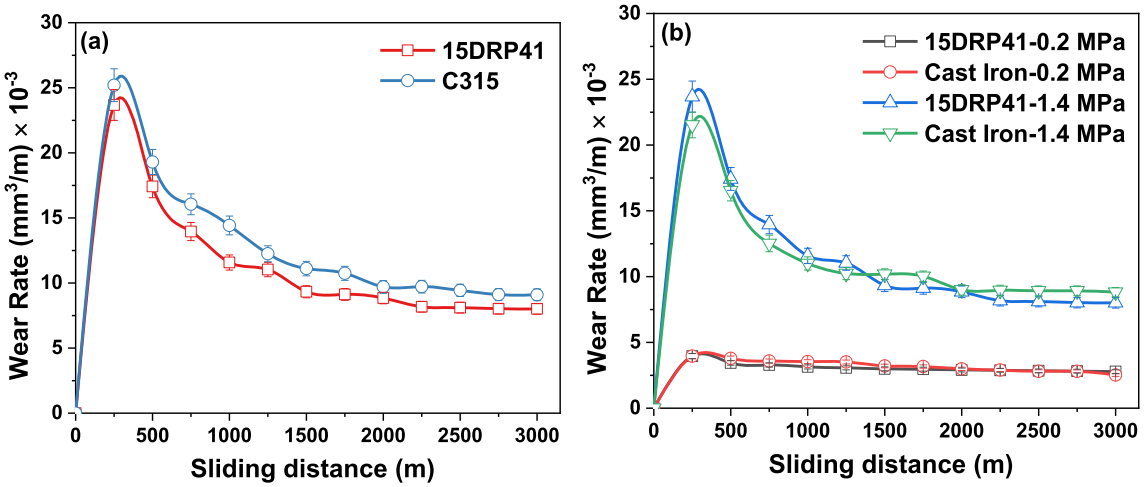

Fig. 7 Comparative wear study of 15DRP41 composite (**a**) C3-15 composite (**b**) cast iron

Table 6 Wear properties of AMCs in comparison with the present study

Authors	Materials	Methods	Hardness (HV)	Density (gm/cm^3)	Average Wear rate* (mm^3/m) × 10^{-3}			
					Contact pressure (MPa)			
					0.2	0.6	1.0	1.4
Arora et al. [9]	LM13+15 wt% dual size rutile	Stir casting	150	-	1.89	4.87	9.01	-
Kumar et al. [2]	LM13+15 wt% $ZrSiO_4$ (Dual size)	Stir casting	116	-	2.01	5.06	8.01	-
Sharma et al. [29]	LM30+15 wt. Sillimanite (3:1; fine: coarse ratio)	Stir casting	-	-	2.68	5.12	7.85	-
Present work	LM30+15wt.% ilmenite (4:1; fine: coarse ratio)	Stir casting	189	3.17	2.53	4.66	6.33	8.51

All readings have been taken from the graph

(at 1.4 MPa) reduction in COF as compared to LM30 base material. This variation was because of the hard ilmenite reinforcement that resist the abrasive wear losses of the pin surface. Thus, the composites prepared shows lower COF than the base material. The COF of 15DRP41 AMC and automobile grade cast iron was observed to be 0.42 and 0.50 at the 1.4 MPa contact pressure. The COF of 15DRP41 AMC is ~ 15% higher than the cast iron as observed.

3.7 Wear Tracks and Wear Debris analysis

The information of the worn surface of 15DRP41 AMC at 0.2 and 1.4 MPa contact pressure is displayed in Fig. 9(a-c). At 0.2 MPa contact pressure, the narrow grooves parallel to the sliding direction with a small delaminated surface area is observed (Fig. 8a). These grooves and craters (delaminated surface) indicate that abrasion and delamination wear

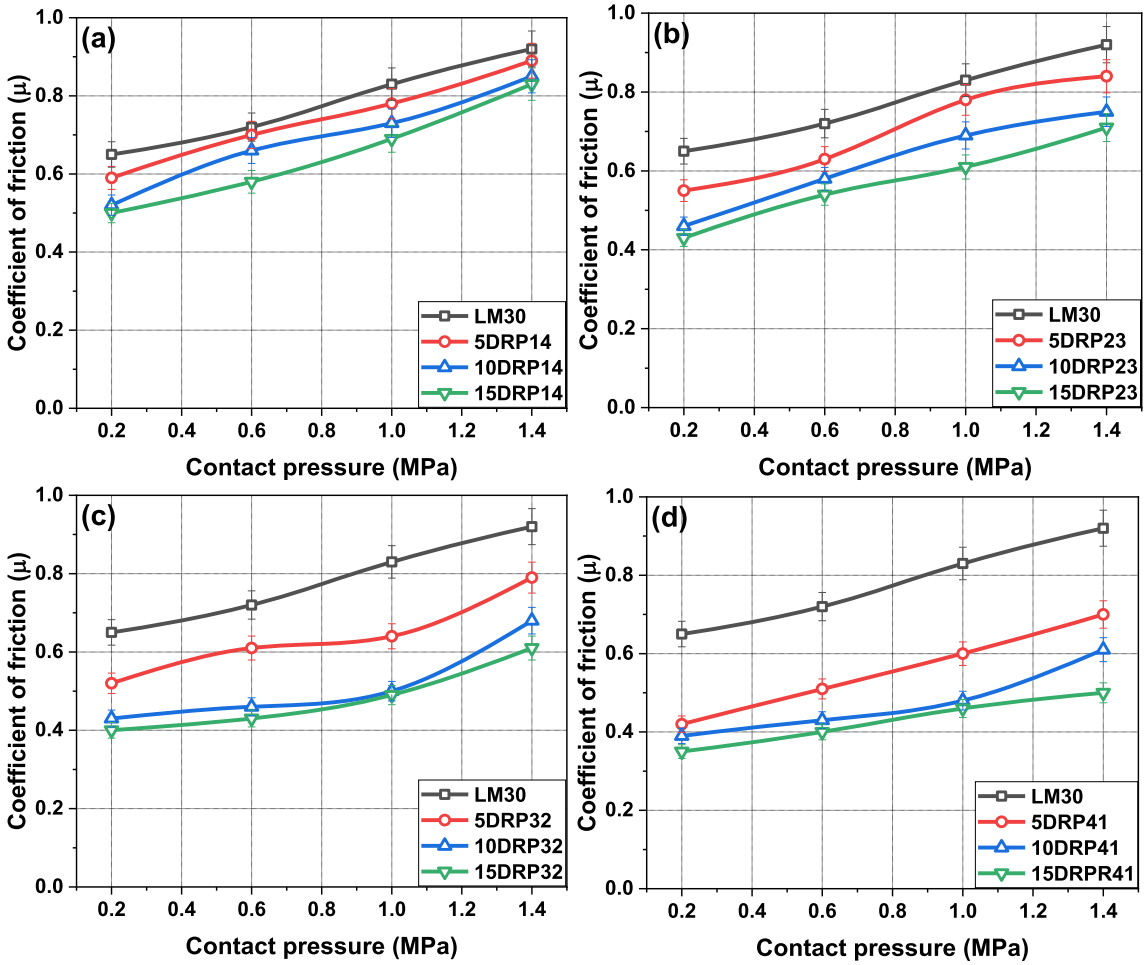

Fig. 8 Represents the coefficient of friction for base alloy and various composites under different contact pressure conditions at same sliding distance

mechanisms dominate. Furthermore, the presence of micro debris on the worn surface indicates that some debris are trapped between the sample and steel disc during sliding action. Figure 9(b, c) shows the worn surface under the contact pressure of 1.4 MPa. Figure 9(b, c) revealed the existence of wide grooves on the worn surface. The contact area of asperities increases due to the deformation of asperities at 1.4 MPa contact pressure. Figure 9(c) shows the extruded surface and microcracks. These microcracks further propagate and join each other leading to the material removal in the form of a sheet.

Further, the SEM images of wear debris are shown in Fig. 9(d-e) at 1.4 MPa contact pressure. Most of the debris are in sheet form, as shown in Fig. 9d. Also, some groove marks on the sheet is observed indicating the abrasive wear mechanism. The adhesive wear mechanism was responsible for the generation of majority of the sheet type debris. In addition, some other types of debris are also observed, like

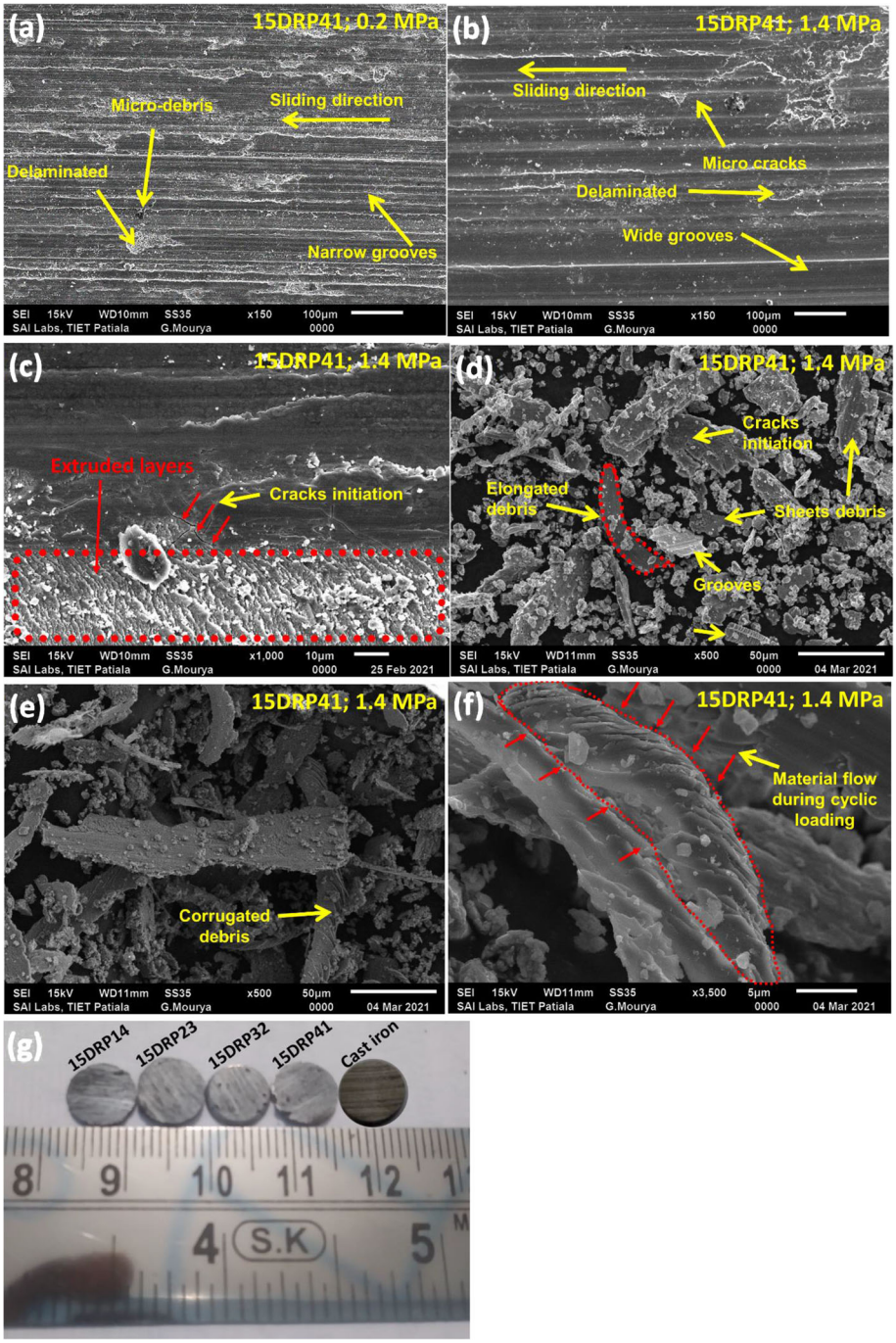

Fig. 9 SEM analysis of (**a**, **b** and **c**) wear track at 0.2 MPa and 1.4 MPa, (**d**, **e** and **f**) wear debris at 0.2 MPa and 1.4 MPa contact pressure, (**g**) Wear track images of prepared samples

micro-crack debris, elongated and corrugated, as shown in Fig. 9(d, e). The cause of the micro-crack is plastic deformation under the applied contact pressure (Fig. 9d) [2]. Thus, under the continuous shear stress acting on the sample surface, wear debris of corrugated shape, as shown in Fig. 9e is observed [27]. Figure 9f shows that the material flow has occurred under the cyclic loading. The stress concentration at a reinforcement junction or oxide particle is more causing crack nucleation. As the sample underwent different stress cycles, numerous parallel ridges built up around the crack initiation site and radiated outwards from it. These ridges were identified as beach marks, a classic indicator of fatigue wear.

Figure 10a shows the EDX spectra of the wear track of the synthesized 15DRP41 AMC at 1.4 MPa contact pressure. The chemical elemental analysis shows different elements like Al, Si, Fe, and O, etc. The presence of oxygen verified the oxidation of the wear surface due to increasing contact temperature at high contact pressure. In this order pin surface interacted with the steel counter surface leading to the transfer of Fe, forming an MML on the subsurface. It played a dynamic role in enhancing the wear resistance of synthesized composites [38]. Consequently, the wear resistance of the 15DRP41 AMC was increased. Figure 9(g) shows the images of wear track of all samples at 68.67 N load.

Figure 10(b-c) presents an EDX analysis of the wear debris of synthesized composite 15DRP41 at 1.4 MPa contact pressure. The spectrum shows that O, Al, C, and Fe are generally the main elements under the action of high contact pressure, as observed from Fig. 10(b-c). It shows that the abrasive wear mechanism was dominant at the beginning of the sliding. Further, the EDS spectrum shows the presence of Fe and O due to the interaction of steel disk surface to pin surface after increasing the contact pressure up to 1.4 MPa. It indicated the formation of MML and confirmed the adhesive wear mechanism.

3.8 Cross-sectional Study of Wear Track Sample

The SEM investigation of the wear track cross-section of sample 15DRP41 is shown in Fig. 11. SEM study showed presence of three-layers beneath the wear surface. The first layer is compacted wear debris containing counter disc material, and

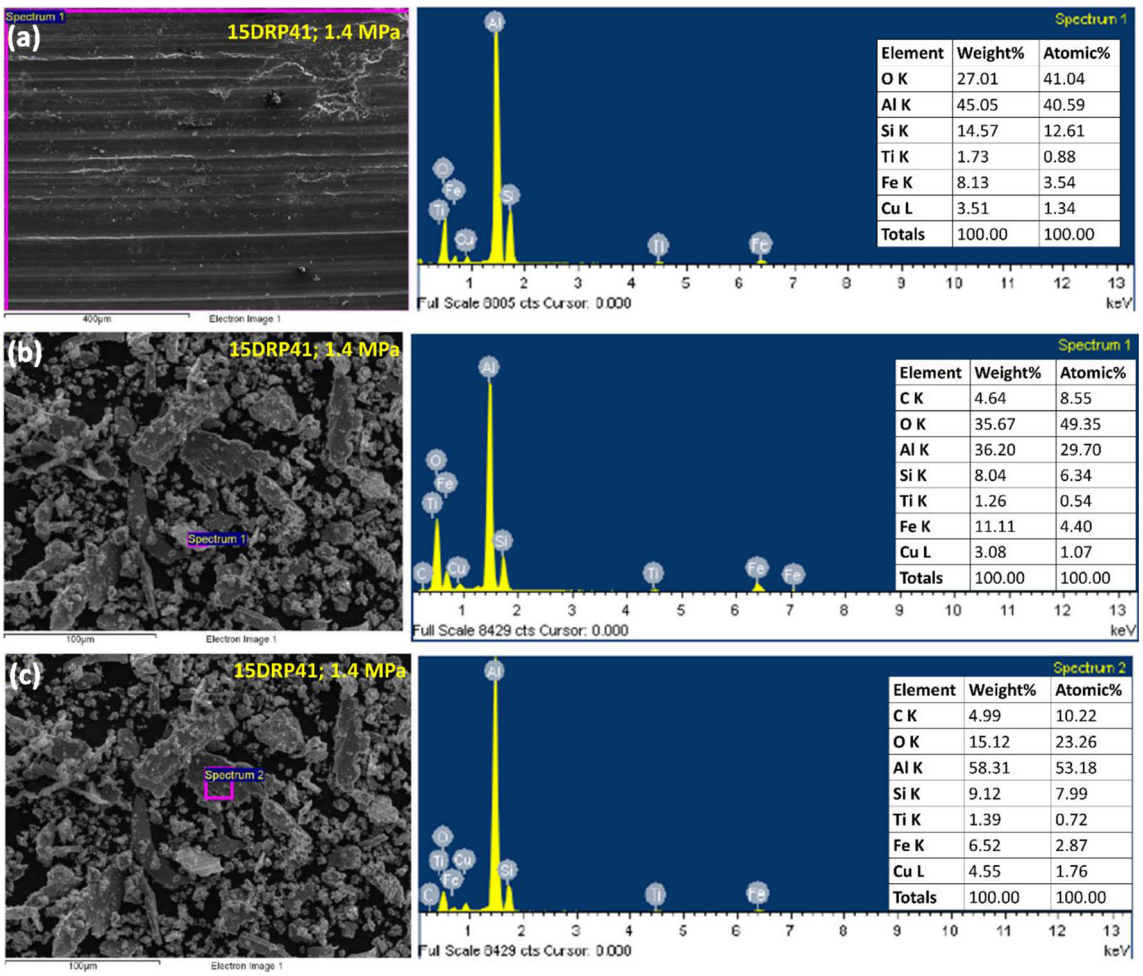

Fig. 10 EDS analysis of 15DRP41 (**a**) wear track, and (**b**, **c**) wear debris at MPa contact pressure

also various oxides that dominate in the tribolayer due to continuous sliding motion and crushing. There are few cracks observed under the wear track. The high hardness of the tribolayer reduces the transformation of shear force beneath the material. In addition, due to the formation of tribolayer, transition in wear rate under continuous sliding also occurs. The thickness of the tribolayer is around 21 μm. Below, the tribolayer a deformed layer was observed in the direction of sliding motion and below this un-deformed composite layer is observed.

The area profile of tribolayer is shown in Fig. 11. The area profile revealed the presence of Al, O, Fe, and Si are major elements. The presence of Fe indicates the transfer of counter disc material on the pin surface. Moreover, O indicates the formation of Al, Si, and Fe oxides.

4 Conclusions

The present work demonstrates the successful fabrication of dual particle ilmenite reinforced AMCs for wear application. Some crucial findings from the study are given below.

- Dual particle range ilmenite reinforcement has shown uniform distribution of particles all over the Al-matrix. Also, with the increased reinforcement, the refinement of Si morphology has increased.
- Microhardness measured at different areas has shown better interfacial strength between the particles and matrix. Furthermore, there was a considerable improvement in the bulk hardness of AMCs.
- The wear rate and COF of fabricated AMCs decreased with the increased ilmenite concentration. Furthermore,

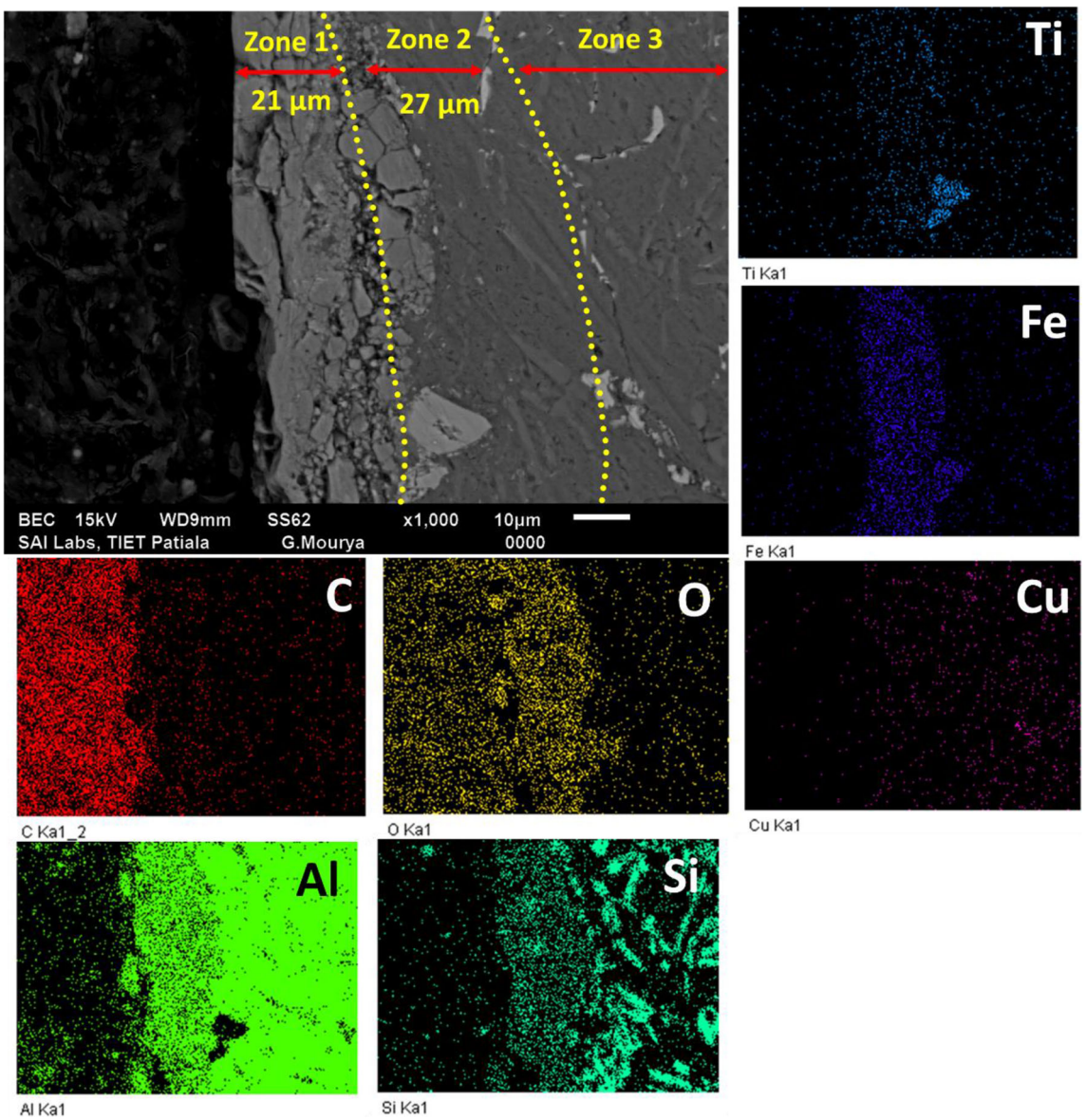

Fig. 11 Cross sectional study of 15DRP41 worn surface at 1.4 MPa contact pressure (**a**) SEM micrograph, (**b**) Elemental area profile

the enhanced fine-to-coarse particle ratio in the AMCs samples reduces the wear rate and COF. The best performance was obtained with 15DRP41 AMC.

- SEM analysis of wear track and wear debris demonstrated that abrasive and adhesive wear mechanism was dominating factor.
- Among all the developed composites 15DRP41 AMC has shown high hardness, wear resistance, and a lesser COF. In addition, the 15DRP41 AMC samples has shown a decrement of ~ 57% in wear rate and ~ 14% in COF than the base material (LM30). The overall wear resistance of the 15DRP41 composite is nearly 7% less at 1.4 MPa contact pressure when compared with the commercial cast iron sample used for break drum application. Thus, the fabricated composites are economical, lightweight material and a better substitute for the replacement of cast iron brake rotors used in automobile industries.
- When compared with single size fine particles reinforced ilmenite composite [26], 15DRP41 composite has shown an improvement of 12% in wear resistance, and 23% in COF. It can be concluded that the dual range reinforcement exhibits better wear and friction properties than the single size particle reinforced composite.

Acknowledgment Author (VS) thanks Dr. Aayush Gupta for valuable suggestions in drafting the manuscript.

Author Contribution Varun Singhal: Conceptualization, design of study, data optimization, analysis, manuscript writing. O. P. Pandey: Results analysis, manuscript writing.

Data Availability All the data and material incorporated in the present manuscript will be made available whenever required.

Declarations Formal consent is not compulsory for the above type of work.

Consent to Participate Authors does not performed any studies involving human or animal participation.

Consent for Publication Consent was got from all individual authors included in the study to publish data.

Disclosure of Potential Conflict of Interest Authors do not have any conflict of interest.

References

1. Yang D, Qiu F, Zhao Q, Wang L, Jiang Q (2017) The abrasive wear behavior of Al2014 composites reinforced with Ti5Si3-coated SiCP. Tribol Int 112:33–41. https://doi.org/10.1016/j.triboint.2017.03.022
2. Kumar S, Sharma V, Panwar RS, Pandey OP (2012) Wear behavior of dual particle size (DPS) zircon sand reinforced aluminum alloy. Tribol Lett 47:231–251. https://doi.org/10.1007/s11249-012-9983-y
3. Radhika N, Raghu R (2019) Abrasive wear behavior of monolithic alloy, homogeneous and functionally graded aluminum (LM25/AlN and LM25/SiO2) composites. Part Sci Technol 37:10–20. https://doi.org/10.1080/02726351.2016.1199074
4. Kumar GBV, Pramod R, Sekhar CG, Kumar GP, Bhanumurthy T (2019) Investigation of physical, mechanical and tribological properties of Al6061–ZrO2 nano-composites. Heliyon 5. https://doi.org/10.1016/j.heliyon.2019.e02858
5. Reddy PS, Kesavan R, Ramnath BV (2018) Investigation of mechanical properties of aluminium 6061-silicon carbide, boron carbide metal matrix composite. Silicon 10:495–502
6. Canakci A, Arslan F (2012) Abrasive wear behaviour of B4C particle reinforced Al2024 MMCs. Int J Adv Manuf Technol 63:785–795. https://doi.org/10.1007/s00170-012-3931-8
7. Yilmaz O, Buytoz S (2001) Abrasive wear of Al2O3-reinforced aluminium-based MMCs. Compos Sci Technol 61:2381–2392. https://doi.org/10.1016/S0266-3538(01)00131-2
8. Singhal V, Pandey OP (2021) Dry sliding wear study of solid lubricants and sillimanite-reinforced aluminum alloy composites. J Mater Eng Perform. https://doi.org/10.1007/s11665-021-05975-y
9. Arora R, Kumar S, Singh G, Pandey OP (2015) Effect of applied pressure on the tribological behaviour of dual particle size rutile reinforced LM13 alloy composite. Charact Miner Met Mater 2016:755–62. https://doi.org/10.1007/978-3-319-48191-3_95
10. Sharma SC (2001) The sliding wear behavior of A16061-garnet particulate composites. Wear 249:1036–1045. https://doi.org/10.1016/S0043-1648(01)00810-9
11. Kumar S, Panwar RS, Pandey OP (2012) Tribological characteristics of Aluminium tri-reinforced particles (Al-TRP) composites developed by liquid metallurgy route. Adv Mater Res 585:574–8. https://doi.org/10.4028/www.scientific.net/AMR.585.574
12. Moazami-Goudarzi M, Akhlaghi F (2013) Effect of SiC nanoparticles content and Mg addition on the characteristics of Al/SiC composite powders produced via in situ powder metallurgy method. Part Sci Technol 31:234–240. https://doi.org/10.1080/02726351.2012.715615
13. Das S, Prasad SV, Ramachandran TR (1989) Microstructure and wear of cast (Al-Si alloy)-graphite composites. Wear 133:173–187
14. Singh G, Goyal S (2018) Microstructure and mechanical behavior of AA6082-T6/SiC/B4C-based aluminum hybrid composites. Part Sci Technol 36:154–161. https://doi.org/10.1080/02726351.2016.1227410
15. Mazahery A, Shabani MO (2012) Study on microstructure and abrasive wear behavior of sintered Al matrix composites. Ceram Int 38:4263–4269. https://doi.org/10.1016/j.ceramint.2012.02.008
16. Sanuprava Mohapatra P, Behera SK, Das (2015) Heavy Mineral Potentiality and Alteration Studies for Ilmenite in Astaranga Beach. J Geosci Environ Prot 3:31–37
17. Singhal V, Pandey OP (2021) Wear and friction behavior of gr/sn solid lubricated dual reinforced AMCs. Silicon. https://doi.org/10.1007/s12633-021-01343-6
18. Singh M, Mondal DP, Das S (2006) Abrasive wear response of aluminium alloy–sillimanite particle reinforced composite under low stress condition. Mater Sci Eng A 419:59–68. https://doi.org/10.1016/j.msea.2005.11.056
19. Kumar CAV, Rajadurai JS (2016) Influence of rutile (TiO2) content on wear and microhardness characteristics of aluminium-based hybrid composites synthesized by powder metallurgy. Trans Nonferrous Met Soc China (English Ed 26:63–73. https://doi.org/10.1016/S1003-6326(16)64089-X
20. Singh M, Mondal DP, Modi OP, Jha AK (2002)Two-body abrasive wear behaviour of aluminium alloy – sillimanite particle reinforced composite. Wear 253:357–368

21. Prasad MGA, Bandekar N (2015) Study of microstructure and mechanical behavior of aluminum/garnet/carbon Hybrid Metal Matrix Composites (HMMCs) fabricated by chill casting method. J Mater Sci Chem Eng 03:1–8. https://doi.org/10.4236/msce.2015.33001
22. Sivakumar S, Padmanaban KP, Uthayakumar M (2014) Wear behavior of the Al (LM24)– garnet particulate composites under dry sliding conditions. Proc Inst Mech Eng Part J J Eng Tribol 228: 1410–1420. https://doi.org/10.1177/1350650114541107
23. Zheng KL, Wei XS, Yan B, Yan PF (2020) Ceramic waste SiC particle-reinforced Al matrix composite brake materials with a high friction coefficient. Wear. https://doi.org/10.1016/j.wear.2020.203424
24. Rasidhar L, Ramakrishna A, Rao CS (2013) Experimental investigation on mechanical properties of ilmenite based Al nanocomposites. Int J Eng Sci Technol 5:1025–1030
25. Elwan M, Fathy A, Wagih A, Essa ARS, Abu-Oqail A, EL-Nikhaily AE (2019) Fabrication and investigation on the properties of ilmenite (FeTiO3)-based Al composite by accumulative roll bonding. J Compos Mater 54:1259–1271. https://doi.org/10.1177/0021998319876684
26. Singhal V, Pandey OP (2021) Utilization of natural mineral ilmenite-reinforced composites for the dry sliding application. Int J Met 2. https://doi.org/10.1007/s40962-021-00724-2
27. Sharma V, Kumar S, Panwar RS, Pandey OP (2012) Microstructural and wear behavior of dual reinforced particle (DRP) aluminum alloy composite. J Mater Sci 47:6633–6646. https://doi.org/10.1007/s10853-012-6599-4
28. Kumar S, Panwar RS, Pandey OP (2013) Effect of dual reinforced ceramic particles on high temperature tribological properties of aluminum composites. Ceram Int 39:6333–6342. https://doi.org/10.1016/j.ceramint.2013.01.059
29. Sharma S, Nanda T, Pandey OP (2018) Effect of dual particle size (DPS) on dry sliding wear behaviour of LM30/sillimanite composites. Tribol Int 123:142–154. https://doi.org/10.1016/j.triboint.2017.12.031
30. Gupta R, Sharma S, Nanda T, Pandey OP (2020) Wear studies of hybrid AMCs reinforced with naturally occurring sillimanite and rutile ceramic particles for brake-rotor applications. Ceram Int 46: 16849–16859. https://doi.org/10.1016/j.ceramint.2020.03.262
31. Das S, Prasad SV, Ramachandran TR, Rohatgi PK (1991) Microstructures of cast Al-Si alloys in the presence of dispersed graphite particles. Mater Trans JIM 32:189–194. https://doi.org/10.2320/matertrans1989.32.189
32. Zykova A, Kazantseva L, Popova N, Vorozhtsov A, Kurzina I (2018) Influence of modifying mixtures on Si crystal formation in Al-7%Si alloy. Met (Basel) 8:1–10. https://doi.org/10.3390/met8020098
33. Vijeesh V, Prabhu KN (2014) Review of microstructure evolution in hypereutectic Al-Si alloys and its effect on wear properties. Trans Indian Inst Met 67:1–18. https://doi.org/10.1007/s12666-013-0327-x
34. Prasad DS, Shoba C, Ramanaiah N (2014) Investigations on mechanical properties of aluminum hybrid composites. J Mater Res Technol 3:79–85. https://doi.org/10.1016/j.jmrt.2013.11.002
35. Priyadarshi D, Sharma RK (2016) Porosity in aluminium matrix composites: cause, effect and defence. Mater Sci Ind J 14:19–129
36. Panwar RS, Pandey OP (2013) Study of wear behavior of Zircon sand-reinforced LM13 alloy composites at elevated temperatures. J Mater Eng Perform 22:1765–1775. https://doi.org/10.1007/s11665-012-0383-0
37. Basavarajappa S, Chandramohan G, Mahadevan A, Thangavelu M, Subramanian R, Gopalakrishnan P (2007) Influence of sliding speed on the dry sliding wear behaviour and the subsurface deformation on hybrid metal matrix composite. Wear 262:1007–1012. https://doi.org/10.1016/j.wear.2006.10.016
38. Basavarajappa S, Chandramohan G, Mukund K, Ashwin M, Prabu M (2006) Dry Sliding Wear Behavior of Al 2219/SiCp-Gr Hybrid Metal Matrix Composites. J Mater Eng Perform 15:668–674. https://doi.org/10.1361/105994906X150803
39. Bhowmik A, Dey D, Biswas A (2021) Characteristics study of physical, mechanical and tribological behaviour of SiC/TiB2 dispersed aluminium matrix composite. Silicon. https://doi.org/10.1007/s12633-020-00923-2
40. Poria S, Sahoo P, Sutradhar G (2016) Tribological characterization of stir-cast aluminium-TiB2 metal matrix composites. Silicon 8: 591–599. https://doi.org/10.1007/s12633-016-9437-5